ing the equations of motion about these known solutions to produce a finite-dimensional model which would establish a direct link between theory and experiment, thus permitting one to investigate numerically the onset of chaos. □

Received 7 April; accepted 14 June 1989.

1. Argoul, F. *et al. Nature* **338,** 51–53 (1989).
2. Libchaber, A., Laroche, C. & Fauve, S. *J. Phys., Paris* **43,** L211–L216 (1983).
3. Pfister, G. *Lecture Notes in Physics* **235,** 199–210 (Springer, Berlin, 1985).
4. Tavener, S. J., Mullin, T. & Cliffe, K. A. *J. Fluid Mech.* (in the press).
5. Broomhead, D. S. & King, G. P. *Physica* D**20,** 217–235 (1986).
6. Guckenheimer, J. & Holmes, P. *Nonlinear Oscillations, Dynamical Systems and Bifurcations of Vector Fields* (Springer, Berlin, 1983).
7. Aubry, N., Holmes, P., Lumley, J. L. & Stone, E. *J. Fluid Mech.* **192,** 115–173 (1988).
8. Roux, J. C., Rossi, A., Bachelart, S. & Vidal, C. *Physica* D**2,** 395–403 (1981).
9. Mullin, T., Tavener, S. J. & Cliffe, K. A. *Europhys. Lett.* **8,** 251–256 (1989).

ACKNOWLEDGEMENTS. This work was supported by the SERC under the 'Nonlinear Initiative' (T.M.) and by a CASE award with the Meteorological Office (T.J.P.). We have received support on the signal-processing techniques from D. Broomhead and R. Jones and on the theoretical interpretation of our results from K. A. Cliffe. S. Todd and D. Pottinger gave useful advice on the computer graphics.

A direct link between the China loess and marine $\delta^{18}O$ records: aeolian flux to the north Pacific

Steven A. Hovan*, David K. Rea*, Nicklas G. Pisias† & Nicholas J. Shackleton‡

* Department of Geological Sciences, University of Michigan, Ann Arbor, Michigan 48109-1063, USA
† College of Oceanography, Oregon State University, Corvallis, Oregon 97331, USA
‡ Godwin Laboratory for Quaternary Research, Cambridge University, Cambridge CB2 3RS, UK

MOST studies of Quaternary climates conducted during the past 150 years have focused on glacial sequences, and for the past 25 years marine sediments have provided significant further understanding of glacial and interglacial palaeoclimates. An important goal of palaeoclimatology, however, to link the well-known detailed continental records to marine records of similar resolution, has yet to be realized. The classic loess sequences of China provide an apparently continuous record of continental climate over the past 2.4 million years[1,2]. The oxygen isotope, $\delta^{18}O$, timescale developed from the marine record[3] gives us a global chronostratigraphy of late Pleistocene climates. Previously, it has been suggested in studies of the aeolian component in pelagic sediments that it may be possible to link these two records directly by finding a suitable core from the north-west Pacific downwind from China[4,5]. Here we report the results of such an effort for core V21-146 (Fig. 1) and tie the last 500,000 years of the Chinese loess–soil sequence directly to the $\delta^{18}O$ timescale and, in so doing, refine the dating of regional loess and soil horizons.

The advantage of using oceanic sediments to infer palaeoclimatic conditions of eastern Asia is the reliability and uniformity of the dating techniques for marine sediments. Late Pleistocene variations in $\delta^{18}O$ values in the $CaCO_3$ of benthic foraminifera shells reflect the changing oxygen-isotope composition of the oceans, which is primarily determined by the volume of isotopically light continental glacial ice[6]—the more ice, the greater the ^{18}O concentration in the oceans. The Specmap project[3] has defined the timing of $\delta^{18}O$ variations in the ocean of the past 800 kyr, providing the basic chronostratigraphy for late Pleistocene palaeoclimatology. Furthermore, since the late Pleistocene $\delta^{18}O$ record is a measure of ice volume, palaeoclimatological indications found in oceanic sediments can be directly compared to presumed glacial–interglacial cycles anywhere on Earth.

TABLE 1 Basal age estimates for Xifeng loess sequence.

Unit		Depth (m)	Susceptibility model age[9] (kyr)	Aeolian age (kyr)
S0		1.0	11	12
L1	LL1	4.4	27	33
	SS1	8.2	56	50
	LL2	11.4	71	85
S1		14.2	126	120
L2	LL1	16.4	138	151
	SS1	18.2	147	172
	LL2	20.2	157	187
	SS2	20.8	161	197
	LL3	22.4	173	209
S2	SS1	24.2	216	229
	LL1	26.4	230	244
	SS2	27.8	251	259
L3		30.9	271	291
S3	SS1	32.0	290	300
	LL1	32.8	302	310
	SS2	34.2	331	336
L4		39.4	361	363
S4		42.6	432	427
L5	LL1	46.8	454	458
	SS1	48.0	463	468
	LL2	49.2	472	476

Loess units and depths from ref. 9.

Many palaeoclimatic studies of eastern Asia have been based on loess[1,2,7], a terrestrial windblown silt deposit[7]. Loess, the most extensive Quaternary sediment in central and northern China, covers over 440,000 km^2, often to depths greater than 200 m. These sequences typically consist of layers of silty loess interbedded with weathered loess or palaeosols. Although these alterations have been ascribed to fluctuating palaeotemperatures or weather patterns[1–8], pedological evidence suggests a closer relationship to the effective soil moisture which controls the nature and density of vegetational cover[9]. Thus, the alternating sequence of loess and soil layers is an indicator of regional precipitation which records oscillations between relatively arid and more humid conditions.

To tie the China loess sequence to other regional and global records of Quaternary climate change, it is important to develop an accurate chronology for the sequence and, if possible, link it to the marine $\delta^{18}O$ record of palaeoclimate. Unfortunately most terrestrial sequences are difficult to date; biostratigraphic and early magnetostratigraphic investigations proved erroneous and unreliable. Recent advances in thermoluminescence,

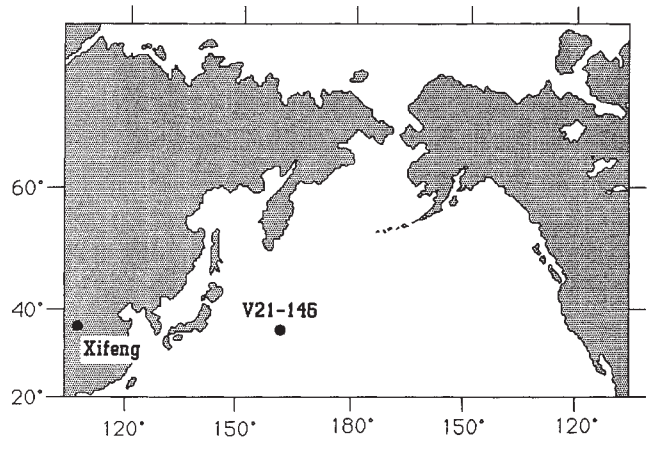

FIG. 1 Map showing the location of Xifeng loess sequence and core V21-146.

palaeomagnetic and radiocarbon techniques have greatly improved dating reliability[10], yet an accurate, high-resolution chronostratigraphy has not been developed. Perhaps the most promising approach is based on the magnetic-susceptibility measurements of loess deposits by Kukla[11], who found that the magnetic susceptibility of loess and interbedded soils varies with the concentration and the grain size of magnetic minerals and increases with the degree of pedogenesis. Kukla assumed a constant deposition rate for magnetic minerals, interpolated between palaeomagnetic reversal horizons and devised a time-scale based on sediment thickness, weighted by susceptibility (Table 1; Fig. 2).

The mass accumulation rate of the aeolian component of oceanic sediments is an indicator of continental climate[5], as shown by the observation that the amount of dust blowing across the north Atlantic is related to the climatic conditions in the Sahara-Sahel source region[12]. Greater annual fluxes of aeolian material occur when conditions are more arid in North Africa[13]. In the north Pacific away from areas of river input and ice rafting, surface sediment mineralogy patterns match those of atmospheric aerosols[14–17], suggesting that wind transport is the primary input mechanism. Pleistocene records of aeolian deposition in the north Pacific contain Milankovitch orbital periodicities[4,18] while longer-term records of aeolian deposition in the region have revealed important changes in aeolian deposition since the Late Cretaceous period[5,19–21]. These studies suggest that aeolian dust composes essentially the entire mineral fraction of the north Pacific pelagic sediments and is a valuable indicator of source-region climate.

To tie the loess sequence of China to the $\delta^{18}O$ chronostratigraphy and palaeoclimatic record we have used core V21-146 (37° 41′ N, 163° 02′ E, 3,968 m; Fig. 1) which provides a continuous record of pelagic sedimentation in the north-west Pacific during much of the late Pleistocene epoch. This site is approximately 2,500 km downwind from mainland China and 3,500 km from the important dust sources in central China[2] (Fig. 1). An oxygen isotope stratigraphy determined from benthic foraminifera was matched to the Specmap standard[3] to develop a detailed chronostratigraphy for this core. An average linear sedimentation rate of ~3.0 cm kyr^{-1} and a sampling interval of 10 cm provided temporal resolution of ~3–4 kyr (Fig. 2). The aeolian component of each sample was isolated by a sequence of chemical extractions[22]. Since this method does not remove volcanogenic components, visual estimates were made from smear slides of ash in the extracted samples and these percentages subtracted from the total amount of extracted material to give true abundance values of continentally derived dust. To avoid the masking of any palaeoclimatic signal because of dilution by other, commonly biogenic, sedimentary components, dust fluxes are expressed as mass accumulation rates mg cm^{-2} kyr^{-1}.

The formation of mid-latitude loess occurs during the glacial periods of the Plio-Pleistocene epochs[7,10]. Since loess forms in semi-arid conditions during times of glaciation[9], maximum fluxes of aeolian dust to the north-west Pacific should coincide with late Pleistocene glaciations[5]. This is the pattern we have found in V21-146 with flux maxima at about 28, 69, 137, 185, 271, 343 and 473 kyr (Fig. 3). Using Kukla's ages[2], we observe a correlation between the deposition of loess layers in China and greater accumulation of aeolian material in the deep sea. The gradual increase of oceanic aeolian fluxes over the past 500 kyr (Fig. 3) apparently reflects a trend toward greater aridity

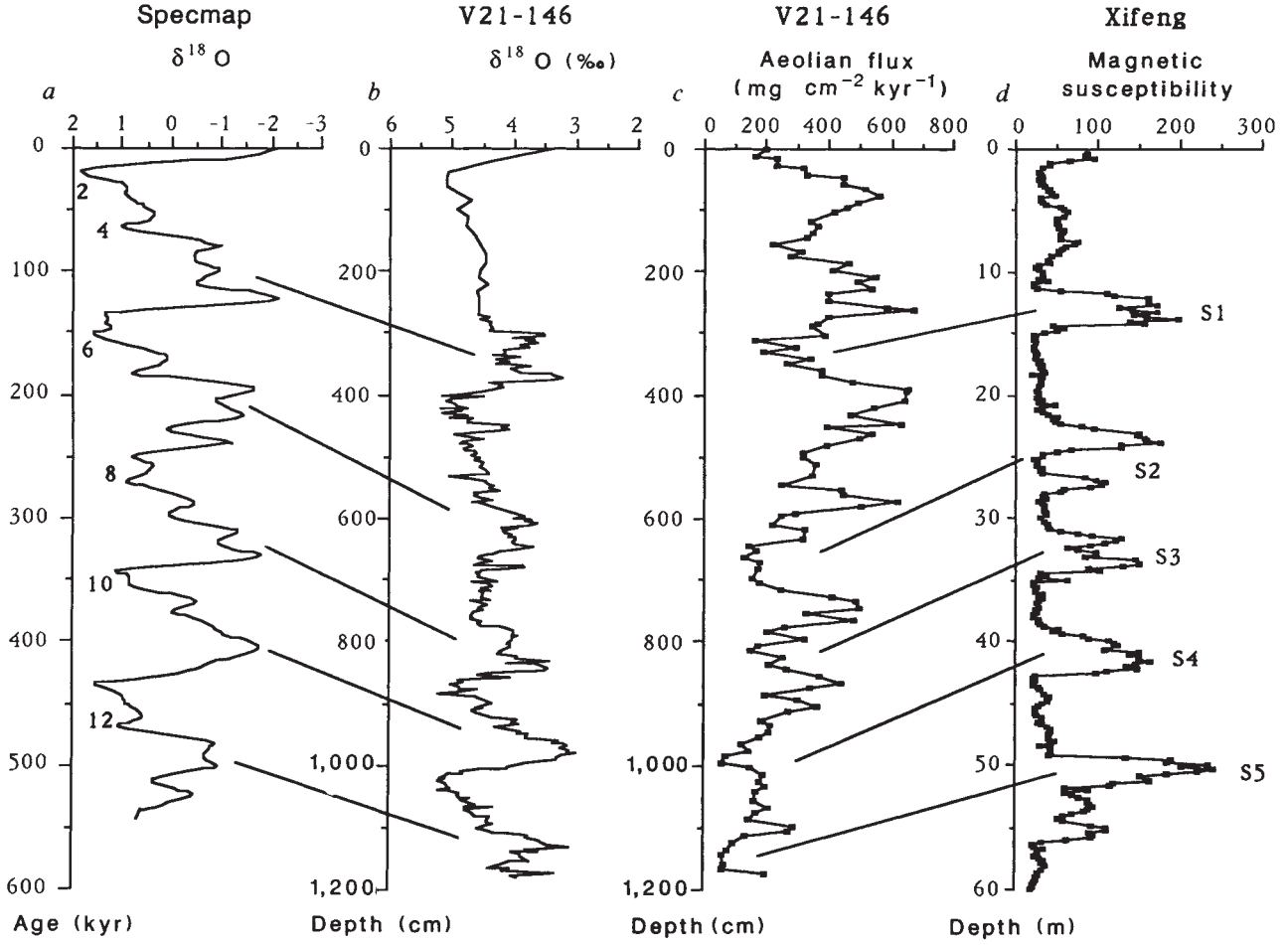

FIG. 2 *a*, Specmap oxygen isotope standard[3]. *b*, Oxygen isotope stratigraphy for V21-146. *c*, Detailed stratigraphy of aeolian deposition in the north Pacific for the past 530 kyrs. *d*, The magnetic susceptibility of the Xifeng loess sequence, which displays an approximate inverse correlation to North Pacific aeolian flux with high-susceptibility palaeosols coinciding with reduced rates of dust deposition in V21-146.

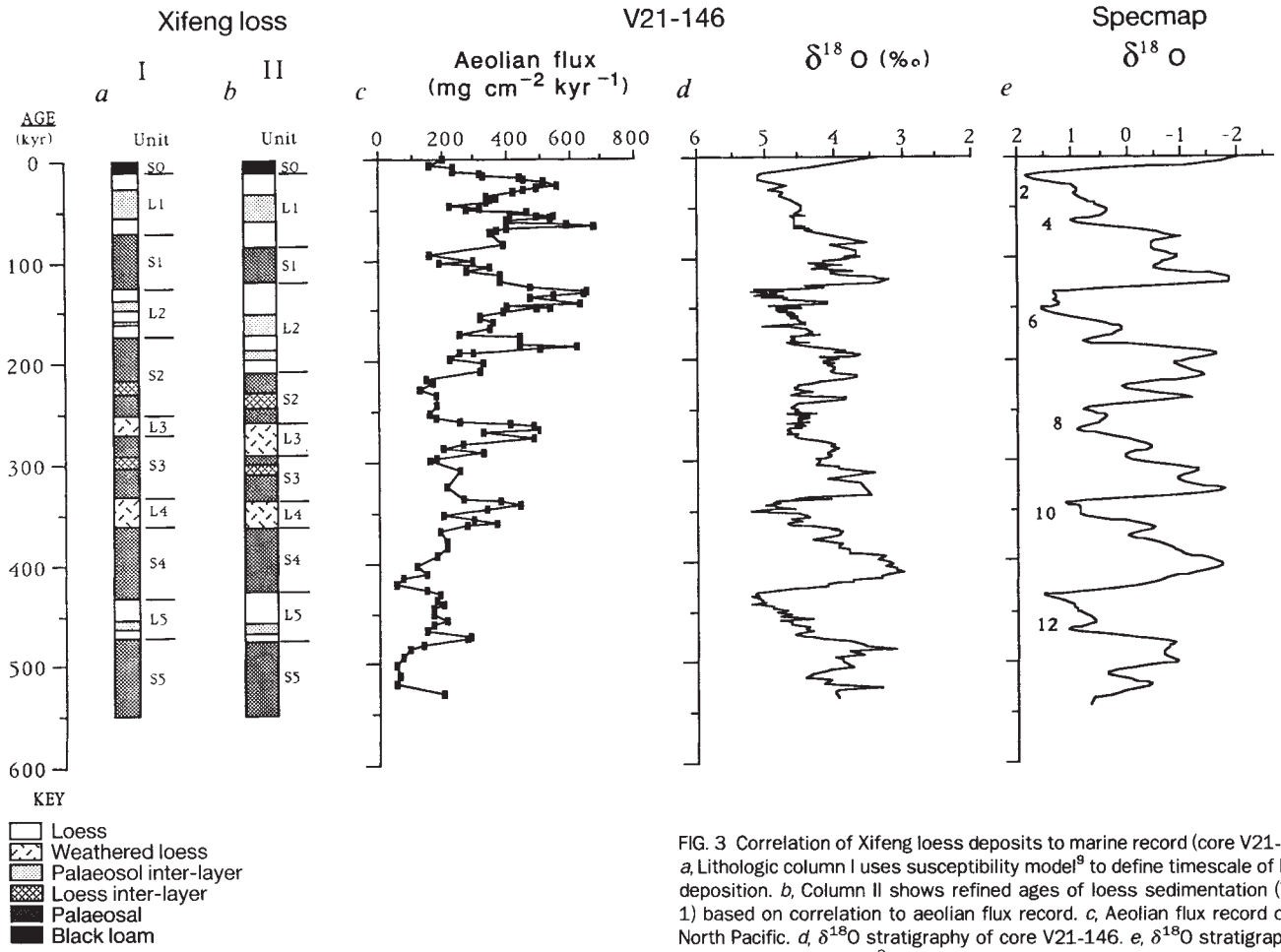

FIG. 3 Correlation of Xifeng loess deposits to marine record (core V21-146). *a*, Lithologic column I uses susceptibility model[9] to define timescale of loess deposition. *b*, Column II shows refined ages of loess sedimentation (Table 1) based on correlation to aeolian flux record. *c*, Aeolian flux record of the North Pacific. *d*, δ^{18}O stratigraphy of core V21-146. *e*, δ^{18}O stratigraphy of Specmap global record[3].

of the climate system in eastern Asia during the late Pleistocene epoch. Similar inferences have been drawn by Pye and Li[8] from observations of increased rates of dust accumulation in the Xifeng loess sequence.

The high-quality aeolian record observed in V21-146 can be linked directly to the loess-soil sequence in Xifeng[9] and to the δ^{18}O timescale[3] (Fig. 3). Combining the accuracy for the δ^{18}O timescale (3–5 kyr) (ref. 3) with the temporal resolution in V21-146 of 3–5 kyr allows age estimates of loess horizons to within ±6 kyr. If we then refine loess-soil ages on the basis of the aeolian correlation model (Table 1), the age span of loess layers L1 and L2 is expanded and the age span of soils S1 and S2 is reduced. Only minor changes are made to older horizons, and in general, the agreement between age assignments made on the basis of the susceptibility model and on our aeolian correlation model is good (Fig. 3). □

Received 3 April; accepted 16 June 1989.

1. Liu T. S. *et al. Loess and the Environment* (Ocean, Beijing, 1985).
2. Kukla, G. *Quat. Sci. Rev.* **6,** 191–219 (1987).
3. Imbrie, J. *et al.* in *Milankovitch and Climate, Understanding the Response to Orbital Forcing, Part 1* (eds Berger, A., Imbrie, J., Hays, J., Kukla, G. & Saltzman, B.) 269–305 (Reidel, Dordrecht, 1984).
4. Janecek, T. R. & Rea, D. K. *Quat. Res.* **24,** 150–163 (1985).
5. Rea, D. K., Leinen, M. & Janecek, T. R. *Science* **227,** 721–725 (1985).
6. Shackleton, N. J. *Nature* **218,** 15–17 (1967).
7. Pye, K. *Aeolian Dust and Dust Deposits* (Academic, London, 1987).
8. Pye, K. & Li, P. Z. *Palaeogeogr. Palaeoclimatol. Palaeoecol.* (in the press).
9. Kukla, G. & An, Z. S. *Palaeogeogr. Palaeoclimatol. Palaeoecol.* (in the press).
10. Heller, F. & Liu, T. S. *Nature* **300,** 431–433 (1982).
11. Kukla G. *et al. Geology* **16,** 811–814 (1988).
12. Prospero, J. M., Glaccum, R. A. & Nees, R. T. *Nature* **289,** 570–572 (1981).
13. Prospero, J. M. & Nees, R. T. *Nature* **320,** 735–738 (1986).
14. Ferguson, W. S., Griffin, J. J. & Goldberg, E. D. *J. geophys. Res.* **75,** 1137–1139 (1970).
15. Leinen, M. & Heath, G. R. *Palaeogeogr. Palaeoclimat. Palaeoecol.* **36,** 1–21 (1981).
16. Blank, M., Leinen, M. & Prospero, J. M. *Nature* **314,** 84–86 (1985).
17. Uematsu, M., Duce, R. A. & Prospero, J. M. *J. atmos. Chem.* **3,** 123–138 (1985).
18. Pisias, N. G. & Leinen, M., in *Milankovitch and Climate, Understanding the Response to Orbital Forcing, Part 1* (eds Berger, A., Imbrie, J., Hays, J., Kukla, G. & Saltzman, B.) 307–330 (Reidel, Dordrecht, 1984).
19. Janecek, T. R. & Rea, D. K. *Geol. Soc. Am. Bull.* **94,** 730–738 (1983).
20. Janecek, T. R. *Init. Rep. DSDP* Burcklo, L. H. **86,** 589–603 (1985).
21. Leinen, M. *Init. Rep. DSDP* Burcklo, L. N. **86,** 581–588 (1985).
22. Rea, D. K. & Janecek, T. R. *Init. Rep. DSDP* Vallier, T. L. **62,** 653–659 (1981).

ACKNOWLEDGEMENTS. We thank G. Kukla for tabulations of his magnetic susceptibility data and comments on this manuscript. Samples from V21-146 were provided by the Core Laboratory of Lamont–Doherty Geological Observatory. This work was supported by NSF, Climate Dynamics Program.

High-temperature hydrothermal precipitation of precious metals on the surface of pyrite

A. Starling, J. M. Gilligan, A. H. C. Carter, R. P. Foster* & R. A. Saunders

Department of Geology, The University, Southampton SO9 5NH, UK

A KNOWLEDGE of high-temperature surface chemistry processes is essential to a complete understanding of the genesis of hydrothermal gold deposits and is also of considerable importance to industrial mineral processing. Here we have studied individual pyrite grains separated from four lode-type gold deposits using optical and scanning electron microscopy and looked at the textural relationships of late gold on the surface of the pyrite. The gold occurs as sub-spherical to subhedral, rarely euhedral, grains. In three of the deposits studied, it is variously accompanied by native tellurium, native silver and altaite. Discrete crystals of gold and

* To whom correspondence should be addressed.